An Improved Positioning Algorithm in a Long-Range Asymmetric Perimeter Security System

Kun Liu, Miao Tian, Junfeng Jiang, Jianchang An, Tianhua Xu, Chunyu Ma, Liang Pan, Tao Wang, Zhichen Li, Wenjie Zheng, Meng Xue, Fan Wu, and Tiegen Liu

***Abstract*—In this paper, an improved positioning algorithm is proposed for a long-range asymmetric perimeter security system. This algorithm employs zero-crossing rate to detect the disturbance starting point, and then utilizes an improved empirical mode decomposition to obtain the effective time-frequency distribution of the extracted signal. In the end, a cross-correlation is used to estimate the time delay of the effective extracted signal. The scheme is also verified and analyzed experimentally. The field test results demonstrate that the proposed scheme can achieve a detection of 96.60% of positioning errors distributed within the range of 0– $\pm$ 20 m at the sensing length of 75 km, which significantly improves the positioning accuracy for the long-range asymmetric fence perimeter application.**

***Index Terms*—Asymmetric dual Mach–Zehnder interferometer (ADMZI), empirical mode decomposition (EMD), fiber optic distributed sensor, positioning algorithm, signal analysis.**

I. Introduction

As a new type of passive distributed sensing system distributed fiber optic sensing system is widely used in long-distance pipelines invasion, leak detection, border security, and other fields, etc. [1]–[8]. With the rapid development of optical fiber sensing technology, fiber security systems have been generated based on dual Mach-Zehnder interferometry (DMZI) vibration detection. Compared with the traditional security systems, the security system based on DMZI has the advantages of high sensitivity, anti-electromagnetic interference and low loss, etc. The key technology of obtaining disturbance position in Asymmetric Dual Mach-Zehnder Interferometer (ADMZI) systems is the positioning algorithm. Currently many cases have been reported regarding the positioning accuracy of the DMZI.

Yang An *et al*. proposed the use of cross-correlation function to estimate the arrival time difference of the two channels disturbance signals, together with applying simulated annealing as the control algorithm to reduce the locating error, which was not only complex to operate and difficult to implement, but also increased the cost of the system [9]. One study by Q. Chen *et al*. significantly improved the computational speed by using the zero-crossing method for detecting vibration starting point and extracting effective data components before the general cross-correlation function. Although the positioning accuracy is 20 m, the range is not large enough in some place [6]. Xie *et al*. used a Butterworth high-pass filter (HPF) to broaden the 3-dB bandwidth of the power spectrum of interference signal, and achieved a smaller locating mean square error (MSE) in the system [5], [10]. Although Xie's algorithm analyzed and reduced the positioning error of DMZI sensor, it ignored the environment noise in the perimeter security.

In order to solve the problems existing in the current equipment such as large positioning error, this paper theoretically analyzes the positioning error of the ADMZI sensing system. Based on the analysis of the theory, we propose an improved positioning algorithm with a low positioning error. Firstly, we achieve endpoint detection with the highest zero-crossing rate (ZCR) as the ZCR is easy and efficient to implement [11], [12]. Meanwhile, in order to obtain a valid signal disturbance and to reduce the computation time, we process the signal based on an improved empirical mode decomposition (EMD) method [13] which uses the correlation coefficient significant test to discard the low test value intrinsic mode function (IMF) components and reconstructs the rest of the signal. Finally, cross-correlation is used to estimate the time delay based on the reconstructed signals [14], [15]. Compared to the other reported positioning algorithms, experimental results verify that our scheme has improved a higher positioning accuracy and achieved a smaller positioning error.

II. Schematic of the ADMZI Vibration Sensor and Positioning Principle

The structure of an ADMZI by using two DFB (distributed feedback) lasers and matching DWDM (dense wavelength division multiplexing) [16] is shown in Fig. 1, where the two outputs of the lasers (λ_1 and λ_2) are equally split by couplers C2 and C3, respectively, then λ_1 and λ_2 propagate in opposite directions in the ADMZI. In clockwise (CW) MZI, the λ_1 interfere with itself at the C3 after being split by C2. The propagation path of

Manuscript received June 14, 2016; revised August 27, 2016; accepted October 3, 2016. Date of publication October 5, 2016; date of current version November 1, 2016. This work was supported in part by the National Natural Science Foundation of China under Grant 61475114, Grant 61405139, Grant 61227011, Grant 61378043, and Grant 61505138, in part by the National Instrument Program under Grant 2013YQ030915, in part by the National Basic Research Program of China under Grant 2010CB327806 and Grant 2010CB327802, and in part by the Tianjin Science and Technology Support Key Project under Grant 11ZCKFGX01900. *(Miao Tian and Kun Liu contributed equally to this work. Miao Tian and Junfeng Jiang are both correspoding authors)*

K. Liu, M. Tian, J. Jiang, C. Ma, T. Wang, Z. Li, W. Zheng, M. Xue, F. Wu, and T. Liu are with the College of Precision Instrument and Opto-electronics Engineering and Key Laboratory of Opto-electronics Information Technology, Ministry of Education, Tianjin University, Tianjin 300072, China (e-mail: 675515611@qq.com; beiyangkl@tju.edu.cn; jiangjfjxu@tju.edu.cn; tgliu@tju.edu.cn).

J. An and L. Pan are with the College of Precision Instrument and Opto-electronics Engineering, Tianjin University, Tianjin 300072, China (e-mail: 55608869@qq.com; anderson.p.l@msn.com).

T. Xu is with the Department of Electronic and Electrical Engineering, University College London, London WC1E 6BT, U.K. (e-mail: tianhua.xu@ucl.ac.uk).

Color versions of one or more of the figures in this paper are available online at http://ieeexplore.ieee.org.

Digital Object Identifier 10.1109/JLT.2016.2615646

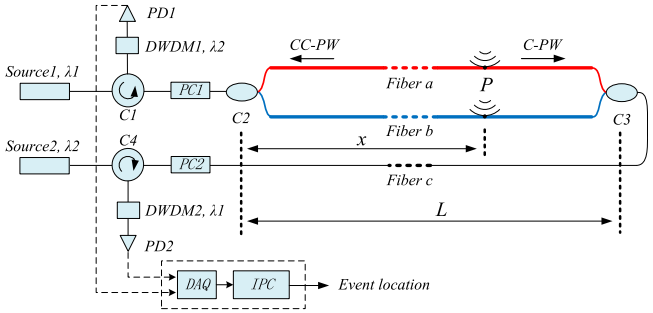

Fig. 1. Schematic diagram of ADMZI disturbance sensing system. C2, C3: 3dB fiber coupler; C1, C4: Optical circulator; PD1, PD2: Photo-detector; PC1, PC2: Polarization Controller; DWDM1, DWDM2: dense wavelength division multiplexers; DAQ: Data Acquisition Card; IPC: Industrial Personal Computer; C-PW, CC-PW: the clockwise and counter-clockwise propagated primary wave.

the λ_1 passes though C1-C2-C3-C4, and is filtered by DWDM1 and detected by PD2 (photo-detector). As DWDM2 can remove the C-RB (clockwise propagated Rayleigh backscattering wave) noise of λ_2 and let the C-PW (clockwise propagated primary wave) of λ_1 go through perfectly, we can easily acquire the signal of C-PW with a high SNR (signal to noise ratio). Here we use two different wavelengths of λ_1 and λ_2 as the sources that are close to 1550 nm, and the difference between λ_1 and λ_2 are larger than the window separation of 0.8 nm. PC1 (polarization controller) and PC2 are used to compensate the visibility variation in each MZI. The situation in the counter-clockwise (CCW) direction MZI is the same.

Assume that a disturbance is suited at a distance of *x*. From Fig. 1, we can see that the time delay *d* between the distances from *P* to PD1 (CCW) and from *P to* PD2 (CW) is usually different. The time difference *d* can be calculated as:

$$d = n \times (L - 2x)/c \tag{1}$$

where *c* is the velocity of lightwave in vacuum ($3 \times 10^8\ m/s$), *n* is the effective refractive index of fiber optic core, *L* is the length of the test cable. Here, *c*, *n* and *L* are all constant. From equation (1), we can deduce the disturbance position *x* from the time delay *d*.

However, there are different kinds of noises in ADMZI in practical applications, the AC components of the received noise-involved interference signal can be expressed as [5], [6]: equation (2) as shown at the bottom of the page.

where *l(t)* is the OPD (optical path difference) generated by vibration, λ_1 and λ_2 are the wavelengths of source1 and source2 in the two MZIs. Polarization effect induces the visibility noise $n_{a1}(t)$, $n_{a2}(t)$ and the phase noise $n_{\varepsilon 1}(t)$, $n_{\varepsilon 2}(t)$. The slight vibration induces the additional environment noise $\xi_1(t)$ and $\xi_2(t)$ in the system. $n_{p1}(t)$ and $n_{p2}(t)$ are the phase noise introduced by the frequency noise of the laser source, $n_{c1}(t)$ and $n_{c2}(t)$ are the additive circuit noise, respectively, $n_{b1}(t)$ and $n_{b2}(t)$ are the back-scattering noise coming from the mixture of

Fig. 2. Framework of position algorithm.

interference signals between CC-RB in fiber *a* and *b* as well as the interference between CC-RB and CC-PW in the coherence area.

According to the above analysis, the use of model (1) will lead to an inaccurate time difference *d* and information loss of non-additive noises only with a simple cross-correlation function. The cross-correlation function is usually employed in slowly varying environment where the characteristics of the signal and noise remain stationary only for finite observation time *T* [17]. In order to apply the cross-correlation function, we can add a restriction and make an assumption to solve this issue.

Restriction: In order to assure that the $\xi_1(t)$ and $\xi_2(t)$ are almost constant during the observation time *T* which is the selected signal segment used for cross-correlation function [17], we set each the observation time to a small value.

Assumption: The additive circuit noises $n_{c1}(t)$ and $n_{c2}(t)$ can be regarded as white noise with small amplitude.

On the basis of the above restrictions, as the $n_{p1}(t)$ and $n_{p2}(t)$ can be reduced by utilizing a narrow line-width laser and compensating the length difference between the two interferometer arms, we can neglect the phase noise. The effect of additive circuit noises $n_{c1}(t)$ and $n_{c2}(t)$ can also be neglected. Similarly, we can also adjust polarization state of the light to compensate $n_{a1}(t)$ and $n_{a2}(t)$, $n_{\varepsilon 1}(t)$ and $n_{\varepsilon 2}(t)$ [18]–[20]. Although the sensing range is long in the ADMZI structure, the SNR still stays high and the RB noise can be suppressed easily, which means the RB noise $n_{b1}(t)$ and $n_{b2}(t)$ can be neglected [16].

Therefore, the alternating current components of the two output signals can be simplified as:

$$\begin{cases} I_1(t) = \cos[2\pi \times \frac{l(t)}{\lambda_2} + \xi_1(t)] \\ I_2(t) = \cos[2\pi \times \frac{l(t-d)}{\lambda_1} + \xi_2(t)] \end{cases} \tag{3}$$

From the equation (3), we can see $I_1(t)$ and $I_2(t)$ are cosine functions. *l(t)* and *l(t-d)* are both functions depending on time *t* only. So, the frequencies of $I_1(t)$ and $I_2(t)$ are proportional to the frequencies of *l(t)* and *l(t-d)* respectively. We can utilize the time-frequency distributions for the $I_1(t)$ and $I_2(t)$ instead of *l(t)* and *l(t-d)* to compute the time delay *d*. $\xi_1(t)$ and $\xi_2(t)$ are constant.

III. Principle of the Proposed Positioning Algorithm

Fig. 2 shows the consequence frame of the positioning algorithm. Firstly, we extract the endpoint of the disturbance signal based on zero-crossing technique. Then we use the improved empirical mode decomposition (EMD) method to discard the low test value IMF components and to reconstruct the rest of

$$\begin{cases} I_1(t) = [1 + n_{a1}(t)] \cdot \cos[2\pi \times \frac{l(t)}{\lambda_2} + \xi_1(t) + n_{\varepsilon 1}(t) + n_{p1}(t)] + n_{b1}(t) + n_{c1}(t) \\ I_2(t) = [1 + n_{a2}(t)] \cdot \cos[2\pi \times \frac{l(t-d)}{\lambda_1} + \xi_2(t) + n_{\varepsilon 2}(t) + n_{p2}(t)] + n_{b2}(t) + n_{c2}(t) \end{cases} \tag{2}$$

the signal. Finally, the cross-correlation is used to estimate the time delay using the reconstructed signals.

A. Endpoint Detection Based on ZCR

ZCR is usually applied to discrete-time signals such as distinguishing the sounds of different frequencies [12]. ZCR can be expressed as:

$$ZCR_n = \sum_{-\infty}^{\infty} |\mathrm{sgn}\,[x(m)] - \mathrm{sgn}\,[x(m-1)]\,|\omega(n-m)$$

$$where \quad \mathrm{sgn}\,[x(n)] = \begin{cases} 1 & x(n) \geq 0 \\ -1 & x(n) < 0 \end{cases}$$

$$and \quad \omega(n) = \begin{cases} 1\ /2N & 0 \leq n \leq N-1 \\ 0 & otherwise \end{cases} \tag{4}$$

Note that *N* is the length of a selected frame. *sgn[x]* is a symbolic function. $\omega(n)$ is a rectangular window function. The principle of signal interception based on ZCR is: the undisturbed signal or noise signal differs from the disturbance signal in frequency domain so that the ZCR of disturbance signal is higher than that of the undisturbed signal or noise signal. Therefore we can pull out the disturbance signal from the undisturbed signal or noise signal easily. In order to improve the robustness of ZCR, it also needs to meet the requirement that vibration amplitude should exceed a certain threshold when the signal is calculated through ZCR. Signal higher than the threshold signal segment is identified as disturbing signal; on the contrary, signal lower than the threshold is regarded as the noise signal or undisturbed signal.

In order to fulfill the assumption and locate the zero-crossing point, we apply the double-threshold crossing method to eliminate the additive circuit noises. As the threshold might truncate the discrete-time signals if the differences between the threshold and successive samples have different algebraic signs. We set the two thresholds as δ_1 and δ_2, where $\delta_1 > 0$, $\delta_2 < 0$, and $|\delta_1| = |\delta_2|$. We note that, in order to eliminate the effect of additive circuit noises, the value of $|\delta_1|$ should be larger than the amplitudes of noise.

And we note that if a point is a zero crossing, it must meet three conditions:

1) The amplitude of the point Z_k *(*$k = 1, 2, 3 \ldots K$*)* is zero.
2) The product of the amplitude of Z_{k-1} (which is before Z_k) and Z_{k+1} (which is after Z_k) is less than zero.
3) The amplitudes of Z_{k-1} and Z_{k+1} cross over the two thresholds δ_1 and δ_2 respectively.

When a point meets the above three conditions at the same time, it can be located as one zero-crossing point. Then we can obtain the endpoint of the disturbance signal from the maximum zero-crossing.

B. An Improved EMD Method

The empirical mode decomposition is a self-adaptive decomposition method based on the local characteristics of the signal, which can effectively decompose the original time-domain signal into the intrinsic mode function with multi-scale time-frequency characteristics. EMD is usually applied to nonlinear and non-stationary processes [21], [22].

Obviously, the disturbance signal of a long range asymmetric perimeter security system is an unsteady signal, which can be decomposed into a collection of IMF components. Each IMF should meet two conditions: (1) in the whole data set, the number of extrema and the number of zero-crossings must either equal or at most have one difference; (2) at any point, both the mean value of the envelope defined by the local maxima and the envelope defined by the local minima are zero.

From the previous EMD algorithm proposed by Huang *et al*. [21], we can only observe the correlation between each IMF component and the original signal qualitatively rather than calculate and compare the degree of correlation quantitatively. In order to calculate the degree of correlation between the original signal and each IMF and to discard the redundant IMF components, we propose an improved EMD which applies the significant test to evaluate the correlation coefficient.

The correlation coefficient is the most common measurement to evaluate the correlation between variables. Generally speaking, the small correlation coefficient means the low correlation between the variables; and vice versa. However, the increase in the length of signals makes the correlation coefficient become lower and the error get larger. Therefore it is obviously inaccurate to only apply the correlation coefficient to evaluate the correlation between investigated signals. Alternatively, we apply *t* test which is one of the significant test of correlation coefficient to evaluate the significance of correlation coefficient between the concerned signals based on statistics principles [23]. The steps of the significant test are following:

1) Decompose the vibration signal into a collection of IMFs c_i *(*$i = 1, 2, 3 \ldots M$*)*. Calculate the correlation coefficient ρ_i for each IMF component with the original signal by formula (5):

$$\rho_i = \frac{\sum_{j=1}^{R} (c_{\mathrm{ij}} - \overline{c_i})(x_j(t) - \overline{x(t)})}{\sqrt{\sum_{j=1}^{R} (c_{\mathrm{ij}} - \overline{c_i})^2 \sum_{j=1}^{R} (x_j(t) - \overline{x(t)})^2}} \tag{5}$$

where the *i th* is the IMF component. *M* is the number of the IMF components. *R* is the total number of points.

2) The *t* test value of the correlation coefficient ρ_i is expressed as:

$$t_i = \frac{\rho_i \sqrt{R-2}}{\sqrt{1-{\rho_i}^2}} \tag{6}$$

3) Check the *t* distribution table to obtain the critical value $t_{\alpha/2}$ based on the given significance level α and freedom degrees *(R-2)*. If $|t_i| < t_{\alpha/2}$, ρ_i is considered to be insignificant in statistics, therefore the corresponding IMF components will be eliminated. Otherwise, it is considered to be significant, and corresponding IMF components will be reserved.

Reconstruct the remaining IMF components after sweeping *t* distribution, and we can obtain the time-frequency information of the disturbance signal.

C. Time Delay Estimation Based on Cross-Correlation

Under the aforementioned restriction, as the short observation time, all processes in (3) can be considered as stationary random processes and the environment noise $\xi_1(t)$ and $\xi_2(t)$ are almost constant during the time. Besides, the cable vibration induced by intrusion can also be considered as a simple harmonic oscillation. Therefore the model of (3) can be formed to the cross-correlation signal - noise model (7) [17]:

$$\begin{cases} I_1(t) = s(t) + n_1(t) \\ I_2(t) = s(t+\tau) + n_2(t) \end{cases} \tag{7}$$

where *s(t)* is the delay signal, $n_1(t)$ and $n_2(t)$ are the additive white Gaussian noise. Assuming that *s(t)*, $n_1(t)$, $n_2(t)$ are zero-mean random stationary process, and *s(t)*, $n_1(t)$, $n_2(t)$ are independent, the cross-correlation function between them is approximately zero. We can directly estimate the time delay between the selected signals after obtaining time-frequency information of the disturbance signal. After $I_1(t)$ and $I_2(t)$ calculated based on cross-correlation, we can have:

$$\begin{aligned} R_{I_1 I_2}(t) = &\ R_{\mathrm{ss}}(t+\tau) + R_{s_1 n_2}(t) + R_{s_2 n_1}(t) + R_{n_1 n_2}(t) \\ \approx &\ R_{\mathrm{ss}}(t+\tau) \end{aligned} \tag{8}$$

where $R_{\mathrm{ss}}(t+\tau)$ is the autocorrelation function of *s(t)*. According to the nature of the autocorrelation function, when $t = -\tau$, we can obtain the maximum of autocorrelation function. Therefore the time delay d can be estimated by locating the peak position of cross-correlation function $R_{I_1 I_2}(t)$.

IV. Field Experiments and Analysis

The practical experiment setup is shown in Fig. 1. The length of the sensing cable is 75 km ($L = 75\,\mathrm{km}$) with single mode fibers. The effective refractive index of fiber is 1.5. The two laser sources λ_1 and λ_2 that we need are 1549.95 nm and 1550.74 nm distributed feedback laser respectively with a power of 5 mW and a line-width of 1.7 kHz (corresponding to the coherence length of 176 km). The central wavelengths of DWDM1 and DWMD2 are 1550.12 nm and 1550.92 nm respectively and with the pass-band width of ± 0.22 nm to match λ_1 and λ_2. The two light beams propagate CW directions (C1-C2-C3-C4) and CCW directions (C4-C3-C2-C1) and are detected by two photo detectors (Model 2053, New Focus) respectively. The synchronous sampling rate of DAQ card and the sampling time of a frame signal are set to be $10\,\mathrm{M/s}$ and 0.3 s respectively. We have conducted 500 sets of in-field experiments in the system. The intrusion is generated at the distance $x = -45041\ m$ from the end side coupler 2 by knocking the fence.

A. Endpoint Detection

Firstly, we obtain the endpoint of the vibration signal based on ZCR after the vibration signal is noise-filtered. The vibration signal of knocking cable and disturbance extraction section are shown in Fig. 3(b). And Fig. 3(c) shows the zero-crossing rate distribution of the vibration signal.

Fig. 3(a) and (b) show the undisturbed signal and interference signals. From the figures, it can be seen that the phase change induced by the intrusion event varies much more fiercely than

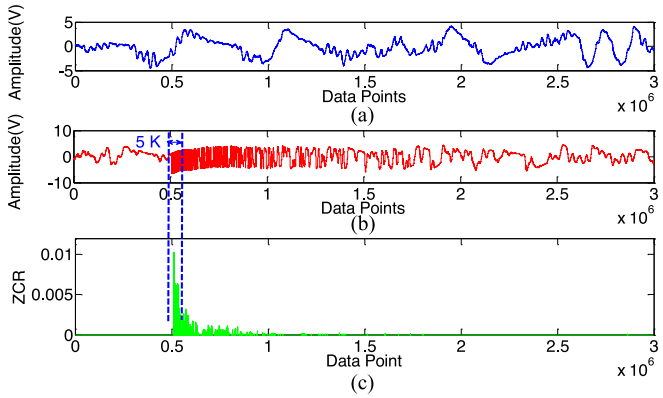

Fig. 3. Undisturbed signal and interference signals. (a) No intrusion. (b) Knocking cable. (c) ZCR of the knocking cable.

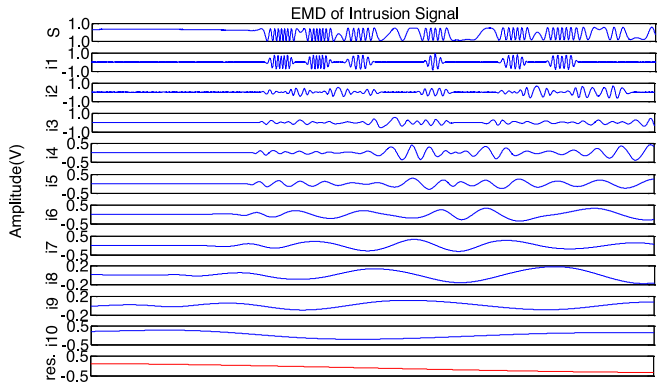

Fig. 4. EMD decomposition.

the environment noise. We can also see different signal densities at different time periods, and the output intrusion signal shows great irregularity. Besides, the large amount of acquisition points will lead to a long time operation if signal is decomposed by EMD subsequently. It is important for selecting a valid signal region.

From Fig. 3(c) we can obtain the zero-crossing rate distribution of the disturbance signal and easily find the peak position of the curve. On the basis of the positioning theory [6], a high ZCR of the signal segment means a large bandwidth with high positioning accuracy. Hence we detect the peak position of the ZCR curve and extract 5 k samples which are around the peak as the effective signal region.

B. An Improved EMD Method

From Fig. 4 we can see the vibration signal is decomposed into IMF components by empirical mode decomposition. The disturbance signal can be expressed as:

$$x(t) = \sum_{i=1}^{M} c_i(t) + r_M(t) \tag{9}$$

From Fig. 4 we can visually see that although each IMF component is decomposed by the original signal, the relevance between each IMF component and the original signal is

TABLE I
CORRELATION COEFFICIENT AND ABSOLUTE VALUE OF T-DISTRIBUTION TEST

IMFs	ρ_i	$\lvert t_i \rvert$
IMF1	0.496	40.402
IMF2	0.388	29.768
IMF3	0.327	24.462
IMF4	0.329	24.652
IMF5	0.231	16.743
IMF6	0.226	16.366
IMF7	0.144	10.317
IMF8	0.127	9.058
IMF9	0.020	1.379
IMF10	–0.014	1.003
res	0.376	28.651

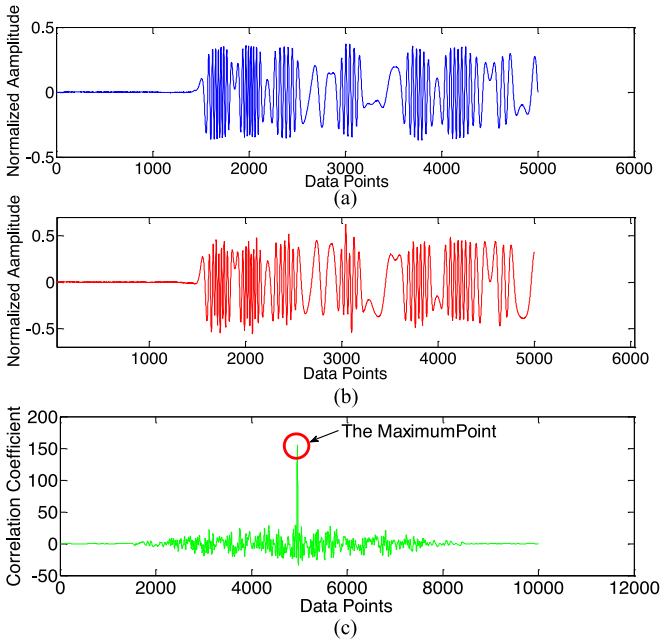

Fig. 5. Reconstruct the signal. (a) One channel signal. (b) Another channel signal. (c) Correlation coefficient of the two channel signal.

different, therefore, the redundant IMF components with a low correlation can be removed.

According to (5), (6), the absolute value of the *t* test $|t_i|$ and the correlation coefficients ρ_i of each IMF are shown in Table I.

We set α to 0.05, $R-2=4998$ and get $t_{\alpha/2}=1.9604$ by checking the *t*-distribution table. Comparing $|t_i|$ to the *t*-distribution at $t_{\alpha/2}=1.9604$, if the former is larger, the corresponding IMF components is retained, otherwise is discarded. Here we eliminate IMF9, IMF10 and reserve the rest. Finally, we reconstruct the disturbed signal by preserving IMF components to obtain the time-frequency information of the disturbed signal, which is shown in Fig. 5(a), (b).

C. Location Based on Cross-Correlation

After reconstructing the disturbed signal based on the improved EMD method we can get time-frequency information of the disturbed signal. In this system, we extract 5 k samples which are around the peak position of the ZCR curve as the effective signal region. The sampling rate of DAQ card is set to be $10\,\mathrm{M/s}$, so the observation time $T=5\times10^3/10\times10^6=0.0005s$. Under the aforementioned restriction, we can apply the cross-correlation signal - noise model of (7) for cross correlation function further. And then the correlation curve of the two channel signal is obtained, which is shown in Fig. 5(c). From Fig. 5(c), we can obtain the time delay estimation by simply using the cross-correlation algorithm.

As a comparison, the experiment based on endpoint detected and cross-correlation (ZCR-CC) without EMD is also conducted. Table II shows position error statistics of 500 sets experiments using the proposed method and ZCR-CC without EMD method.

TABLE II
COMPARISON OF POSITIONING ERROR STATISTICS BETWEEN THE PROPOSED METHOD AND ZCR-CC WITHOUT EMD METHOD

Method	Mean absolute error(MAE/m)	Standard deviation(SD/m)
Proposed Method	4.74	7.74
ZCR-CC without EMD	31.16	52.33

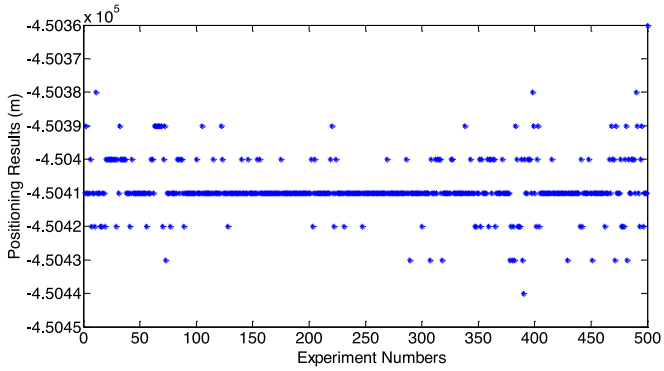

Fig. 6. Experimental results of the 500 sets positioning test by the proposed method.

From the Table II, compared to ZCR-CC without EMD (MAE $=31.16\,\mathrm{m}$, SD $=52.33\,\mathrm{m}$), the proposed method (MAE $=4.74\,\mathrm{m}$, SD $=7.74\,\mathrm{m}$) can achieve the variance of the positioning results is 7.74 m and correspond to an accuracy of 0.01% for the full sensing length of 75 km, which can significantly reduce the SD and MAE of the location error and improve the positioning accuracy in the long range asymmetric fence perimeter system.

Fig. 6 shows the experimental results of the 500 sets positioning test by the proposed method. According to the experimental positioning results, it is shown that compared to the theoretical value of locating -45041 m, the proposed method can detect up to 96.60% of positioning errors distributed within ±20 m. Especially, 84.80% of the location error distributes within ±10 m can be detected, which is very close to the theoretical precision limit. That means that only a minor part of error is outside the range of ±20 m.

V. CONCLUSIONS

This paper proposes an improved positioning algorithm in long range ADMZI vibration sensors. We have theoretically

analyzed the principle of the positioning in the long range optical fiber perimeter security system by taking into account all types of noises. According to the theoretical analysis, we applied ZCR to extract the endpoint of the intrusion signal. Then we used an improved EMD method to eliminate low redundant IMF components and to obtain a valid signal disturbance. Finally, the cross-correlation function was used to estimate the time delay of the reconstructed signals. The field experiments demonstrate that the proposed approach can achieve the detection of 96.60% of positioning errors distributed within the range of $0 \sim \pm 20\,\mathrm{m}$ and the variance of the positioning results is 7.74 m corresponding to an accuracy of 0.01% for the full sensing length of 75 km, which has a good potential in practical long range asymmetric perimeter security systems.

REFERENCES

[1] J. C. Juarez, E. W. Maier, K. N. Choi, and H. F. Taylor, "Distributed fiber-optic intrusion sensor system," *J. Lightw. Technol.*, vol. 23, no. 6, pp. 2081–2087, Jun. 2005.

[2] Y. Liu, L. Wang, C. Tian, M. Zhang, and Y. Liao, "Analysis and optimization of the PGC method in all digital demodulation systems," *J. Lightw. Technol.*, vol. 26, no. 18, pp. 3225–3233, Sep./Oct. 2008.

[3] S. Liang *et al.*, "Fiber-optic intrinsic distributed acoustic emission sensor for large structure health monitoring," *Opt. Lett.*, vol. 34, pp. 1858–1860, Jun. 2009.

[4] S. Xie, M. Zhang, S. Lai, and Y. Liao, "Positioning method for dual Mach–Zehnder interferometric submarine cable security system," *Proc. SPIE*, vol. 7677, pp. 76770A-1–76770A-4, 2010.

[5] S. Xie, Q. Zou, L. Wang, M. Zhang, Y. Li, and Y. Liao, "Positioning error prediction theory for dual Mach–Zehnder interferometric vibration sensor," *J. Lightw. Technol.*, vol. 29, no. 3, pp. 362–368, Feb. 2011.

[6] Q. Chen *et al.*, "An improved positioning algorithm with high precision for dual Mach–Zehnder interferometry disturbance sensing system," *J. Lightw. Technol.*, vol. 33, no. 10, pp. 1954–1960, May 2015.

[7] X. Zhang, T. Liu, K. Liu, J. Jiang, Z. Ding, and Q. Chen, "Reducing location error and processing time of dual Mach–Zehnder interferometric fiber perturbation sensor using zero-crossing analysis," in *Proc. 22nd Int. Conf. Opt. Fiber Sensor*, Oct. 2012, pp. 8421A8-1–8421A8-4.

[8] B. Kizlik, "Fibre optic distributed sensor in Mach–Zehnder interferometer configuration," in *Proc. Int. Conf. Mod. Probl. Radio Eng., Telecommun. Comput. Sci.*, 2002, pp. 128–130.

[9] Y. An, H. Feng, Y. Zhou, S.-j. Jin, and Z.-m. Zeng, "A control method to eliminate polarization-induced phase distortion in dual Mach–Zehnder fiber interferomete," in *Proc. IEEE 2012 United Kingdom Autom. Control Int. Conf.*, 2012, pp. 988–991.

[10] S. Xie, M. Zhang, Y. Li, and Y. Liao, "Positioning error reduction technique using spectrum reshaping for distributed fiber interferometric vibration sensor," *J. Lightw. Technol.*, vol. 30, no. 22, pp. 3520–3524, Nov. 2012.

[11] R. G. Bachu, S. Kopparthi, B. Adapa, and B. D. Barkana, "Separation of voiced and unvoiced using zero crossing rate and energy of the speech signal," in *Proc. Amer. Soc. Eng. Educ. Zone Conf.*, 2008, pp. 1–7.

[12] S. S. Mahmoud and J. Katsifolis, "Elimination of rain-induced nuisance alarms in distributed fiber optic perimeter intrusion detection systems," *Proc. SPIE Defense, Security, Sens.*, vol. 7316, pp. 731604-1–731604-11, 2009.

[13] J. H. Zhang, Y. C. Han, L. Z. Li, J. Liu, and B. Che, "An improved EMD time-frequency analysis method for rocket vibration signal," in *Proc. 2014 IEEE Chin. Guid., Navig. Control Conf.*, 2014, pp. 1842–1846.

[14] I. Cespedes, J. Ophir, and S. K. Alam, "The combined effect of signal decorrelation and random noise on the variance of time delay estimation," *IEEE Trans. Ultrason., Ferroelectr. Freq. Control*, vol. 44, no. 1, pp. 220–225, Jan. 1997.

[15] Y. Rui and D. Florencio, "Time delay estimation in the presence of correlated noise and reverberation," in *Proc. IEEE Int. Conf. Acoust., Speech Signal Process.*, 2004, vol. 2, pp. 133–136.

[16] C. Ma *et al.*, "Long range distributed fiber vibration sensor using an asymmetric dual Mach–Zehnder interferometers," *J. Lightw. Technol.*, vol. 34, no. 9, pp. 2235–2239, May 2016.

[17] C. Knapp and G. Carter, "The generalized correlation method for estimation of time delay," *IEEE Trans. Acoust., Speech Signal Process.*, vol. ASSP-24, no. 4, pp. 320–327, Aug. 1976.

[18] A. D. Kersey, A. Dandridge, and A. B. Tveten, "Dependence of visibility on input polarization in interferometric fiber-optic sensors," *Opt. Lett.*, vol. 13, no. 4, pp. 288–290, 1988.

[19] A. D. Kersey, M. J. Marrone, and A. Dandridge, "Observation of input polarization-induced phase noise in interferometric fiber-optic sensors," *Opt. Lett.*, vol. 13, no. 10, pp. 847–849, 1988.

[20] A. Galtarossa, L. Palmieri, M. Schiano, and T. Tambosso, "Statistical characterization of fiber random birefringence," *Opt. Lett.*, vol. 25, no. 18, pp. 1322–1324, 2000.

[21] N. E. Huang *et al.*, "The empirical mode decomposition and the Hilbert spectrum for nonlinear and non-stationary time series analysis," *Proc. SPIE*, vol. 454, no. 1971, pp. 903–995, Mar. 1998.

[22] Kun Liu *et al.*, "A high-efficiency multiple events discrimination method in optical fiber perimeter security," *J. Lightw. Technol.*, vol. 33, no. 23, pp. 4885–4890, Dec. 2015.

[23] S. You and Y. Yu, *Statistics*. Wuhan, China: Wuhan Univ. Press, 2001, pp. 115–118.

Kun Liu received the B.Eng. degree in opto-electronics information engineering, and the M.Eng. and Ph.D. degrees in optical engineering, in 2004, 2006, and 2009, respectively, all from Tianjin University, Tianjin, China.

From 2009 to 2010, he worked toward the postdoctoral research in Tianjin University, where he is currently an Associate Professor in the College of Precision Instrument and Optoelectronics Engineering. He is also in the Key Laboratory of Opto-electronics Information and Technical Science, Ministry of Education, Tianjin University. His research interest focuses on the development of physics and chemistry sensing system based on optical fiber laser.

Miao Tian was born in Chongqing, China, in 1990. She received the B.Sc. degree from the School of Optical Engineering, Changchun University of Science and Technology, Changchun, China, in 2014. She is currently working toward the M.S degree in optical engineering at Tianjin University, Tianjin, China.

She is a student of Associate Professor Kun Liu. Her research interest mainly focuses on distributed fiber sensing.

Junfeng Jiang received the B.S. degree from the Southwest Institute of Technology, Mianyang, China, in 1998, and the M.S. and Ph.D. degrees from Tianjin University, Tianjin, China, in 2001 and 2004, respectively. He is currently a Professor with Tianjin University. His research interests include fiber sensors and optical communication performance measurement.

Jianchang An, biography not available at the time of publication.

Tianhua Xu, biography not available at the time of publication.

Chunyu Ma, biography not available at the time of publication.

Liang Pan, biography not available at the time of publication.

Tao Wang, biography not available at the time of publication.

Zhichen Li, biography not available at the time of publication.

Wenjie Zheng, biography not available at the time of publication.

Meng Xue, biography not available at the time of publication.

Fan Wu, biography not available at the time of publication.

Tiegen Liu received the B.Eng., M.Eng., and Ph.D. degrees in 1982, 1987, and 1999, respectively, from Tianjin University, Tianjin, China. He is currently a Professor with Tianjin University. His research interests include photoelectric detection and fiber sensing. He is a Chief Scientist of the National Basic Research Program of China.